

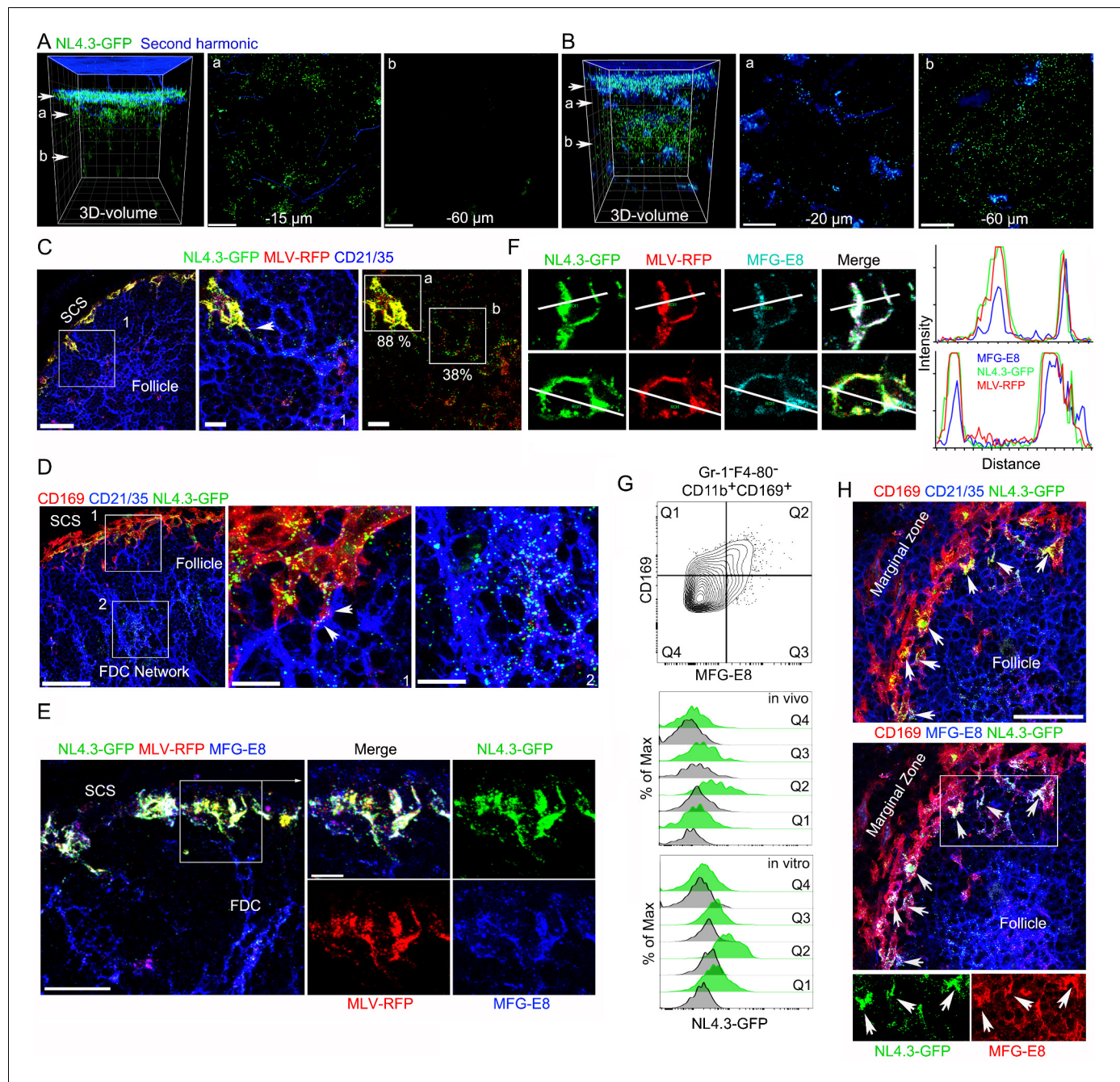


---

## Figures and figure supplements

An integrin/MFG-E8 shuttle loads HIV-1 viral-like particles onto follicular dendritic cells in mouse lymph node

**Chung Park and John H Kehrl**



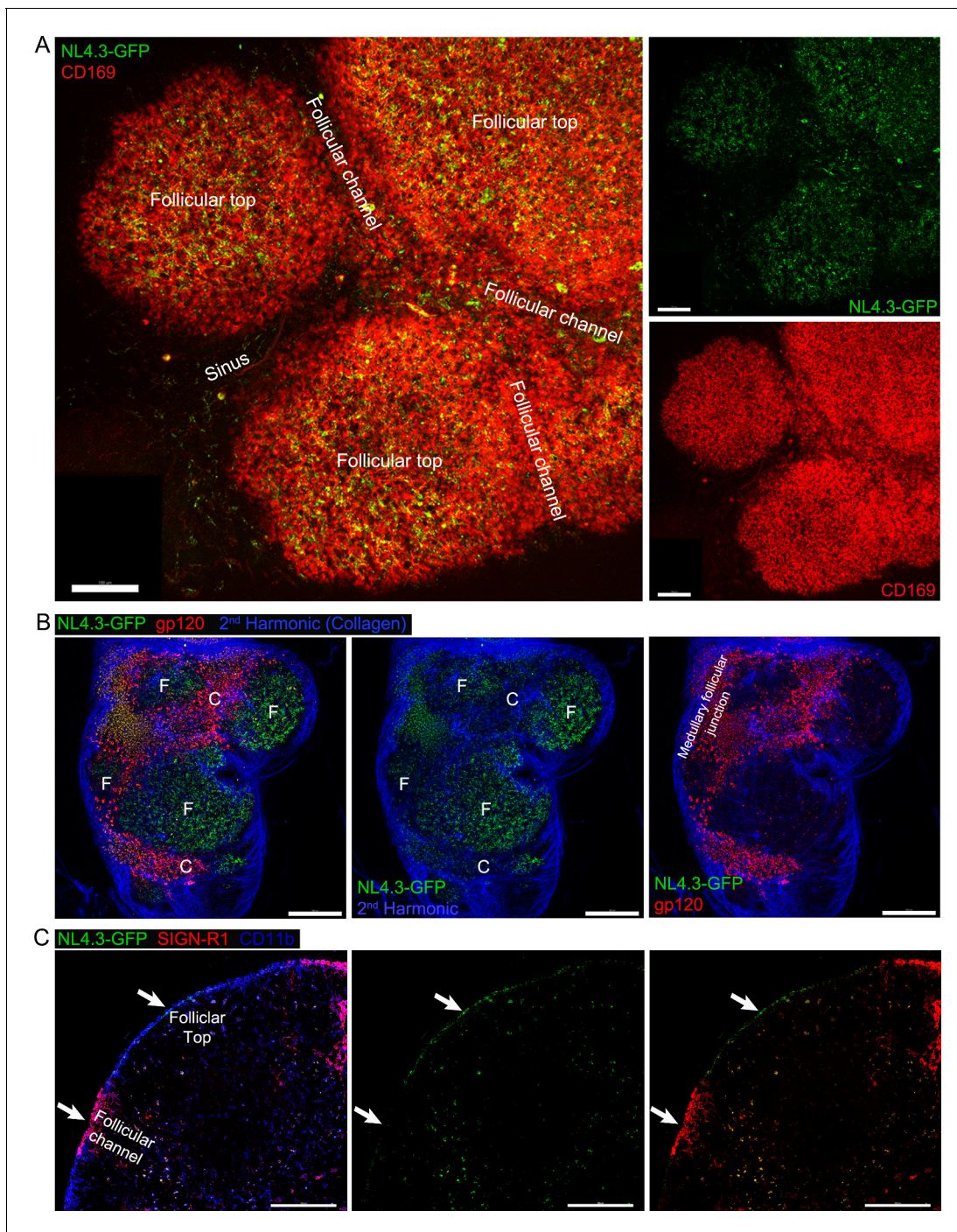
**Figure 1.** VLPs accumulated in MFG-E8<sup>+</sup> compartment in SCSM and on the FDC network. (A, B) LN TP-LSM thick volume micrographs of NL4.3-GFP (green) 6 hr (A) and 20 hr (B) post VLPs injection. LN structure visualized by second harmonic (blue) of capsule and sinus floor. In left panel the top arrow indicates the subcapsular sinus floor and arrow a and b the location of the cross-sectional 10  $\mu$ m volume image shown in panels a and b. Distance from the sinus floor to indicated areas are shown. Grid spacing in volume images is 20  $\mu$ m. Scale bars 20  $\mu$ m. (C) LN confocal micrographs of NL4.3-GFP and MLV-RFP 3 hr post VLPs injection. Box 1 in first panel zoomed in 2<sup>nd</sup> and 3<sup>rd</sup> panels. Arrowhead in 2<sup>nd</sup> panel indicates a contact point between SCSM and FDC. Colocalization scores of NL4.3-GFP and MLV-RFP in SCSM and FDCs are noted. (D) LN confocal micrographs of NL4.3-GFP 8 hr after NL4.3-GFP injection. Boxes in upper panel zoomed in middle and lower panel. Middle panel arrowheads indicate abutment of SCSM and FDC. (E) Confocal micrographs of NL4.3-GFP and MLV-RFP in inguinal LN 3 hr post VLPs injection. FDC networks were visualized with FDC-M1 (MFG-E8) antibody. Box in left panel was electronically zoomed. (F) Two SCSMs were analyzed for the co-localization of NL4.3-GFP, MLV-RFP and MFG-E8. Region of interest (ROI) in each panel are indicated with white lines. Signal intensity in ROIs were plotted. (G) Flow cytometry of LN cells. Gr-1<sup>+</sup>F4-80<sup>-</sup>CD11b<sup>+</sup>CD169<sup>+</sup> population from total LN cells was plotted with MFG-E8 versus CD169, which generated Q1, Q2, Q3, and Q4. Histograms show NL4.3-GFP signal (green) and background control (gray) of indicated populations. Upper, LN cells from NL4.3-GFP injected mice. Lower, purified LN cells incubated with NL4.3-GFP. (H) Spleen confocal micrographs of NL4.3-GFP 6 hr after intravenous VLP injection. Upper panel, FDC networks

Figure 1 continued on next page

*Figure 1 continued*

visualized with CD21/35 and lower panel, FDC networks visualized with MFG-E8 antibody. In bottom panels are shown separated pseudo-colored signals of boxed area in lower panel. NL4.3-GFP (green, left) and MFG-E8 (red, right). Arrows indicate MFG-E8<sup>+</sup> compartment. Scale bars 30  $\mu\text{m}$  and 10  $\mu\text{m}$  (A, B, E), 50  $\mu\text{m}$  (F).





**Figure 1—figure supplement 1.** NL4.3-GFP rapidly localized on SCSMs that overlie the LN follicle rather than those over the interfollicular region. (A) Tiled confocal micrographs of NL4.3-GFP in inguinal LN at 1 hr after injection. SCSMs covered B cell follicle visualized by CD169 (red) antibody injection 30 min before imaging. Left panel, follicular channels are located between B cell follicles. Right upper, NL4.3-GFP signal only. Right lower, CD169 signal only. (B) Tiled TP-LSM thick volume micrographs of NL4.3-GFP (green) and labeled gp120 (red) in inguinal LN. NL4.3-GFP and labeled gp120 simultaneously injected 1 hr before imaging. Collagen capsule of LN was visualized by 2<sup>nd</sup> harmonic signal (blue), left. Collagen and NL4.3-GFP signals, middle panel. Collagen and gp120 signals, right panel. Follicular top (F) and interfollicular channel (C) indicates microstructure of LN that overlie and divide the LN follicle. Medullary follicular junction indicates area between follicular top and medullary. (C) Tiled confocal micrographs of NL4.3-GFP in inguinal LN harvested at 1 hr after injection. Fixed LN section was stained with antibodies of SIGN-R1 (red) and CD11b (blue). Left panel, all signals merged. Middle panel, NL4.3-GFP signal only. Right panel, SIGN-R-1 and NL4.3-GFP signals. Follicular top and follicular channel were indicated by arrows. Scale bars 100  $\mu$ m (A), 200  $\mu$ m (B) and 100  $\mu$ m (C).



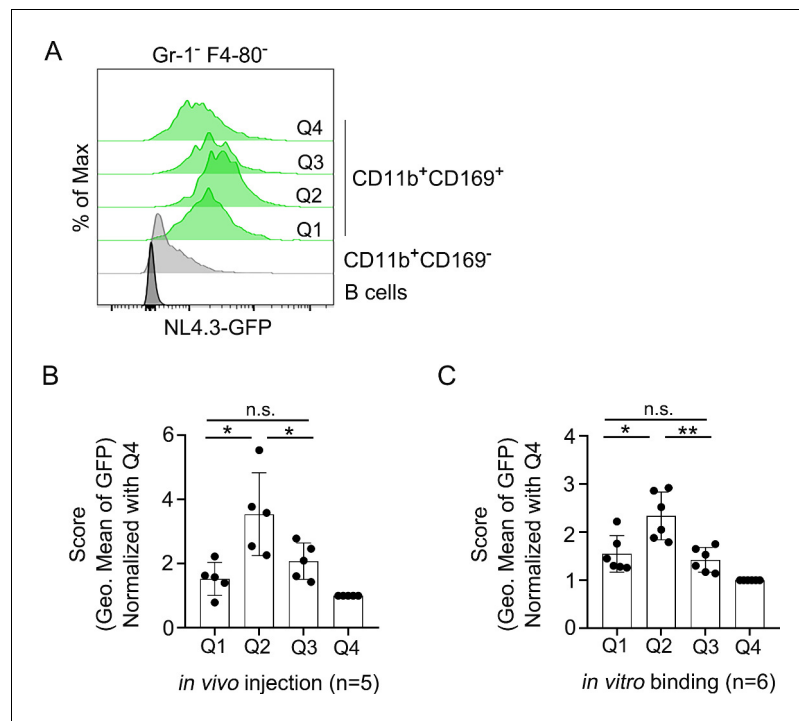


**Figure 1—figure supplement 2.** The lymph node MFG-E8<sup>+</sup> SCSMs capture NL4.3-GFP VLPs. **(A)** Histogram shows NL4.3-GFP signal (green) of indicated populations. GFP signal of CD11b<sup>+</sup>CD169<sup>-</sup> macrophages (gray) and B cells (dark gray) are shown for comparison. **(B)** Level of NL4.3-GFP signal of different populations are shown. The GFP signal strength was normalized to the Q4 population signal. LN cells obtained from 5 mice 3 hr after NL4.3-GFP injection stained and analyzed. **(C)** Purified LN cells from six different mice stained with surface markers after binding of NL4.3-GFP on ice for 30 min. \*,  $p < 0.1$ , \*\*,  $p < 0.01$ .

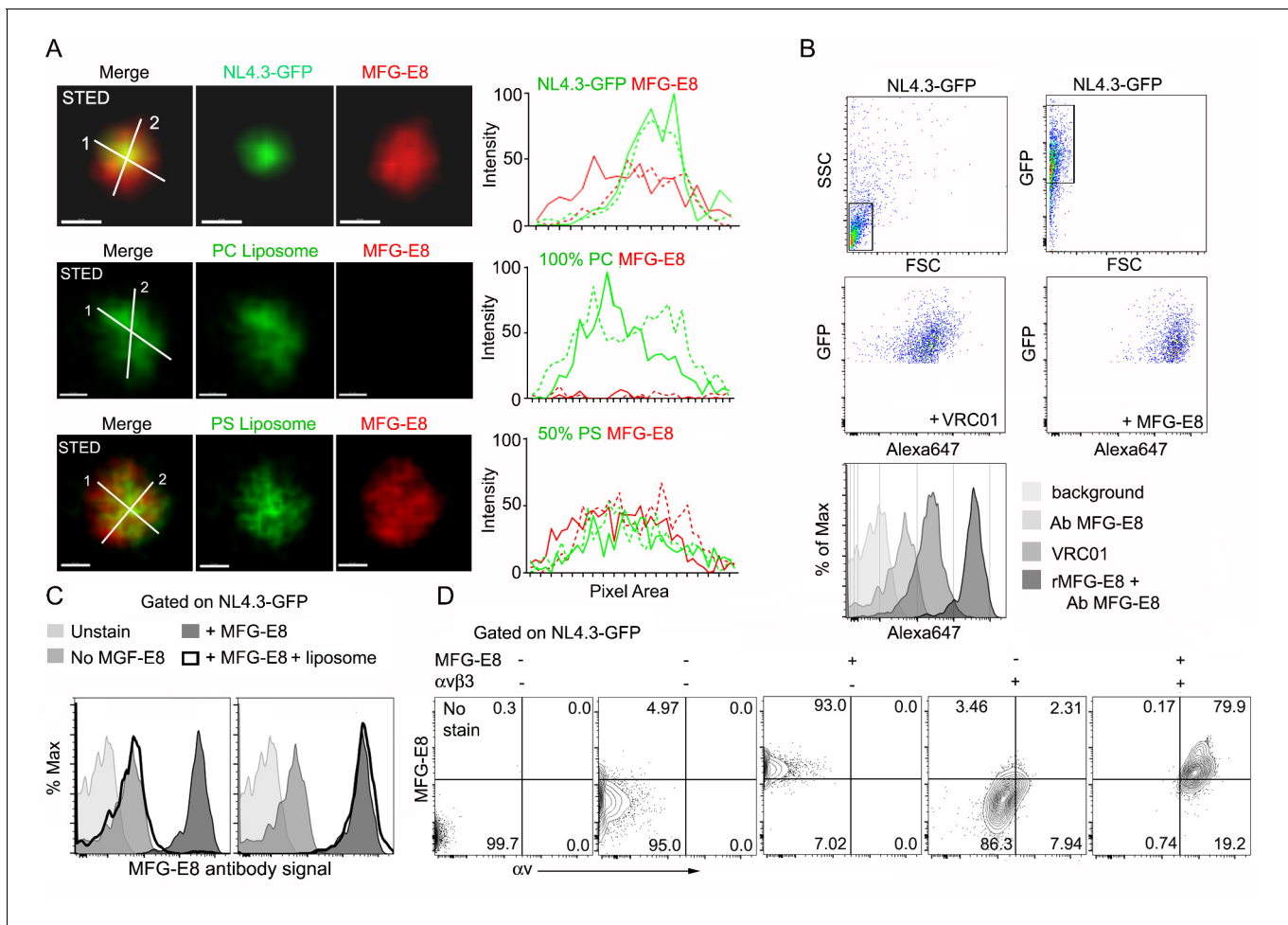


**Figure 2.** HIV-1 VLPs bind MFG-E8, which can interact with  $\alpha v \beta 3$  integrins. (A) STED microscopy images of HIV-1 VLP/MFG-E8 complex (top row), PC-liposome and bound MFG-E8 (middle row), and PS-liposome and bound MFG-E8 (bottom row). Corresponding graphs show signal intensities along axis 1 (solid) and axis 2 (dotted line). Scale bars 100 nm. (B) Flow cytometry analyzing VRC01 and MFG-E8 binding NL4.3-GFP VLPs. FSC versus SSC shown in 1<sup>st</sup> panel. 1<sup>st</sup> panel boxed region used to analyze FSC versus GFP in 2<sup>nd</sup> panel. GFP versus Alexa 647-VRC01, 3<sup>rd</sup> panel; and Alexa 647-MFG-E8, 4<sup>th</sup> panel. NL4.3-GFP VLPs confirmed by VRC01 antibody staining and MFG-E8/NL4.3-GFP complexes detected by MFG-E8 antibody staining and flow cytometry. (C) Flow cytometry detects competitive inhibition of MFG-E8 binding NL4.3-GFP by PS-liposome (left), but not PC-liposome (right). (D) Flow cytometry detects MFG-E8/ $\alpha v \beta 3$  integrin/NL4.3 GFP complexes. Binding of recombinant proteins to NL4.3-GFP detected by  $\alpha v$  and MFG-E8 antibodies.

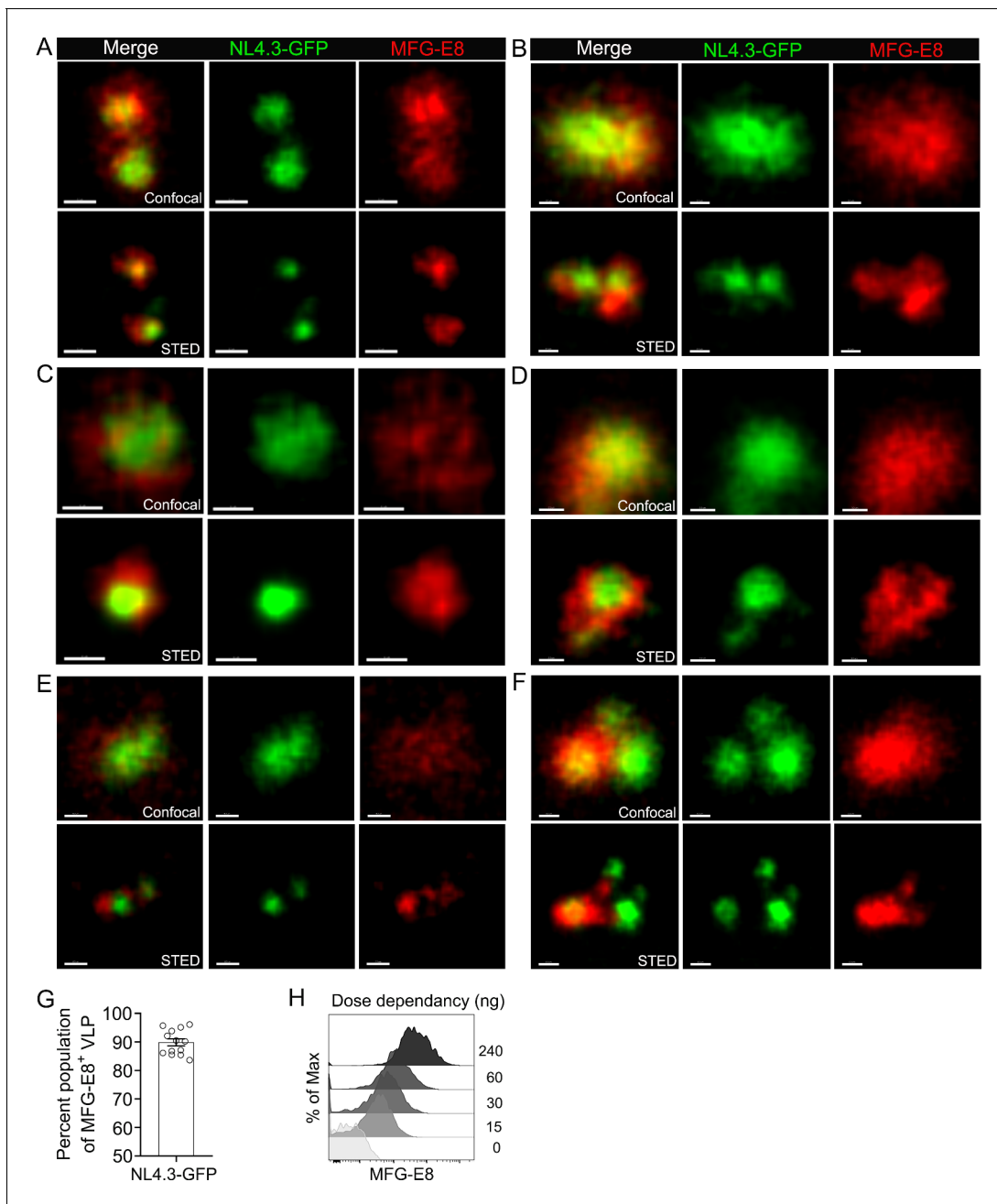


**Figure 2—figure supplement 1.** MFG-E8 encasing NL4.3-GFP VLPs. (A–F) Confocal (upper) and corresponding STED (lower) micrographs of HIV-1 VLP/MFG-E8 complexes. Scale bars 100 nm (A–C), 200 nm (D–F). (G) Percent of HIV-1 VLPs coated with VLP/MFG-E8 complexes were plotted. Percent populations were obtained from 13 separated binding experiments. (H) Histograms shows that dose dependency of MFG-E8 binding to HIV-1 VLP. Directly labeled mouse recombinant MFG-E8 incubated with NL4.3-GFP on ice for 30 min. HIV-1 VLP/MFG-E8 complexes were measured by flow cytometry.



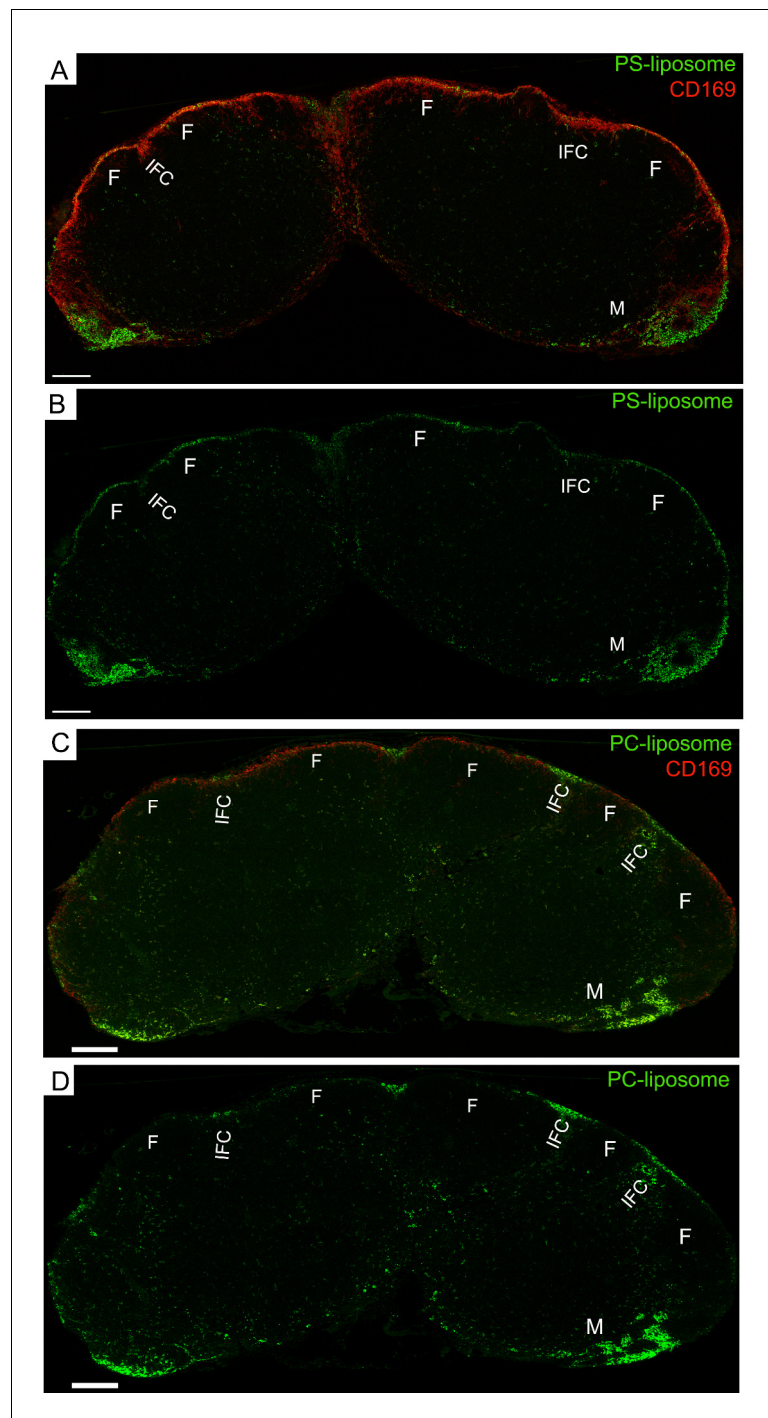


**Figure 2—figure supplement 2.** PS-liposome target SCSMs, while PC-liposome mainly target medullary and interfollicular channel SMs. (A) Tiled confocal micrographs of PS-liposome in inguinal LN harvested 1 hr after liposome injection. B cell follicle (F), interfollicular channel (IFC), and medullary area (M) are indicated. (B) PS-liposome signal only shown. (C) Tiled confocal image of PC-liposome in inguinal LN harvested 1 hr after liposome injection. CD169 immunostained red. B cell follicle (F), interfollicular channel (IFC), and medullary area (M) are indicated. (D) PC-liposome (green) signal only shown. Scale bars 200  $\mu$ m.

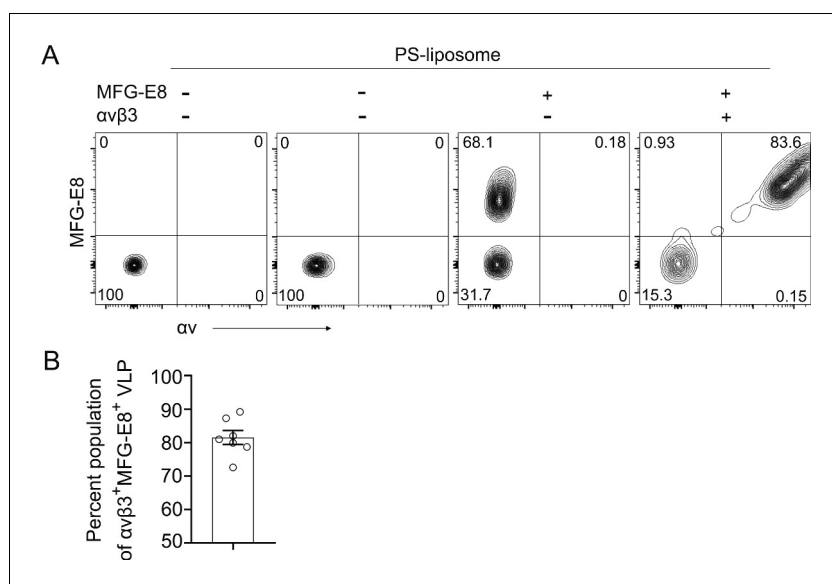


**Figure 2—figure supplement 3.** MFG-E8 bound HIV-1 VLPs bind to integrin  $\alpha\beta3$ . **(A)** Flow cytometry detects MFG-E8/ $\alpha\beta3$  integrin/PS liposome complexes. PS-liposome incubated with directly labeled recombinant MFG-E8 and  $\alpha\beta3$  integrin on ice 30 min. Binding of recombinant proteins to PS-liposome detected by  $\alpha v$  antibody. **(B)** Percentage of HIV-1 VLPs bound to MFG-E8 and  $\alpha\beta3$  integrins shown. Percentages obtained from seven separate binding experiments.

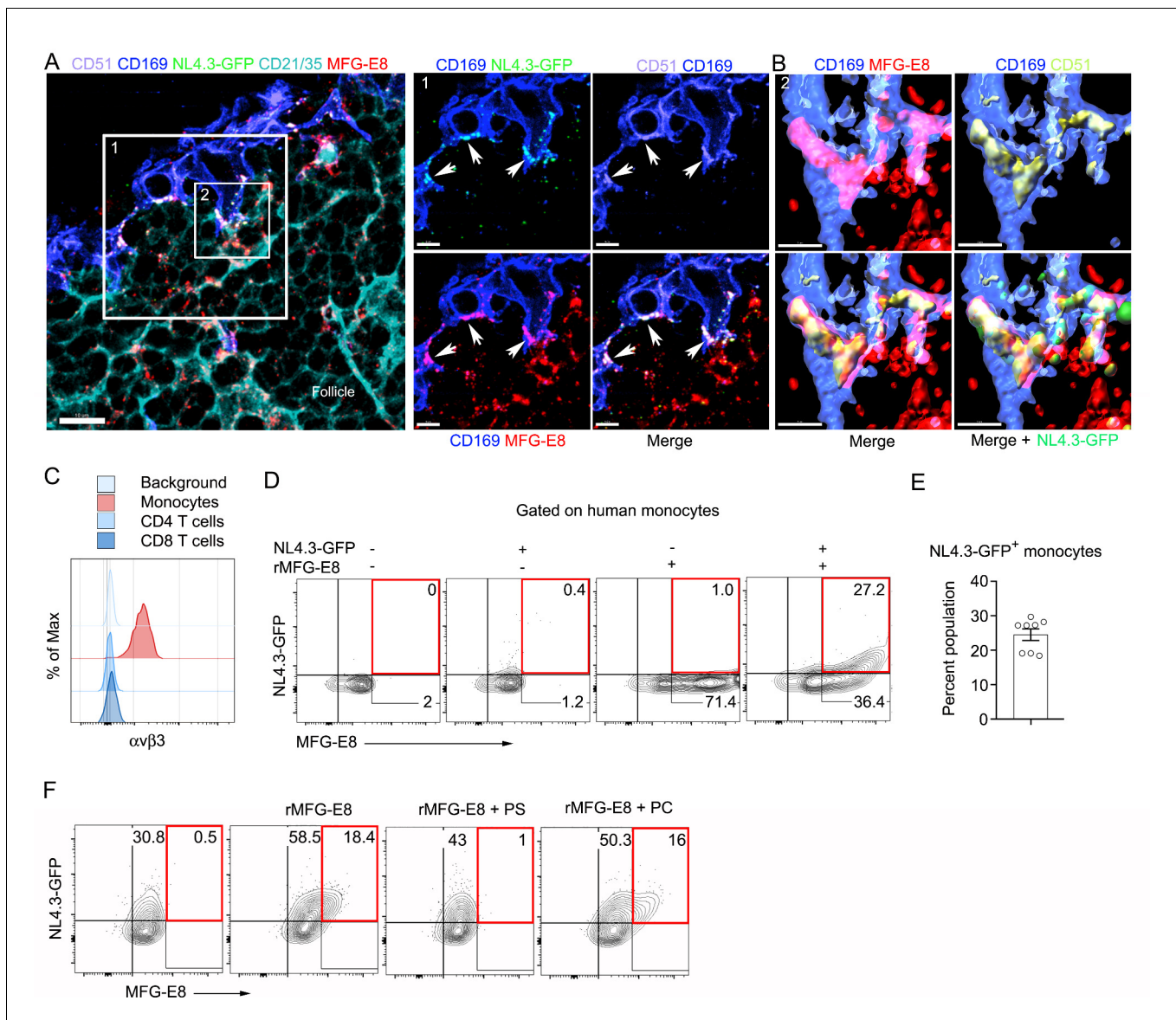


**Figure 3.** MFG-E8 functions as a bridging molecule to target HIV-1 VLPs to murine SCSM and human monocytes. (A) LN confocal micrographs of NL4.3-GFP 3 hr after NL4.3-GFP injection. Box 1 zoomed in right panels. Arrow heads indicate overlapping signals. (B) Box 2 in (A) used for 3D-reconstruction in right panels. Triple signals (CD169, CD51, and MFG-E8) were shown as yellowish compartments in left lower panel. NL4.3-GFP signal was overlapped on the compartment in right lower panel. (C) Flow cytometry detects  $\alpha\beta 3$  integrin expression on human monocytes (CD14<sup>+</sup> PBMC). (D) Addition of recombinant MFG-E8 enhanced NL4.3-GFP binding on human monocytes. Gates were highlighted with red boxes. (E) Percent of NL4.3-GFP<sup>+</sup> population of human PBMC enhanced by recombinant MFG-E8 pretreatment was plotted. Human PBMC from eight individuals were tested by in vitro binding assay. (F) PS-liposome inhibited recombinant MFG-E8 mediated NL4.3-GFP binding on human monocytes. Gates highlighted with red boxes. Scale bars 10 and 5  $\mu\text{m}$  (A), and 2  $\mu\text{m}$  (B).



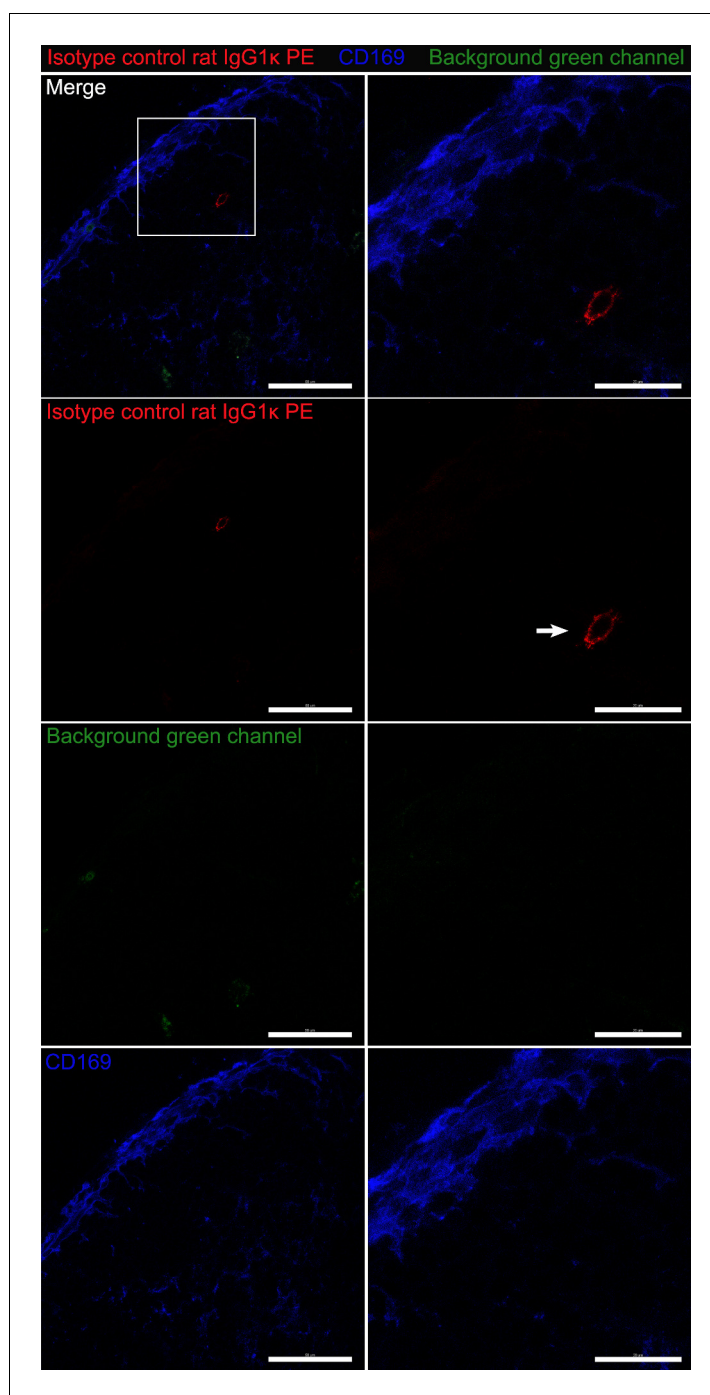


**Figure 3—figure supplement 1.** Confocal images of isotype control for CD51 staining. Confocal micrographs of inguinal LN. Fixed section stained with PE-conjugated rat IgG1<sub>k</sub> isotype control antibody (red) and CD169 antibody (blue). Boxed area electronically zoomed in second column. First row, all signals merged. Second row, red signal only. Third row, green signal only. Fourth row, CD169 signal only. Arrow indicates non-specific signals in red channel. Scale bars 50  $\mu$ m and 20  $\mu$ m.

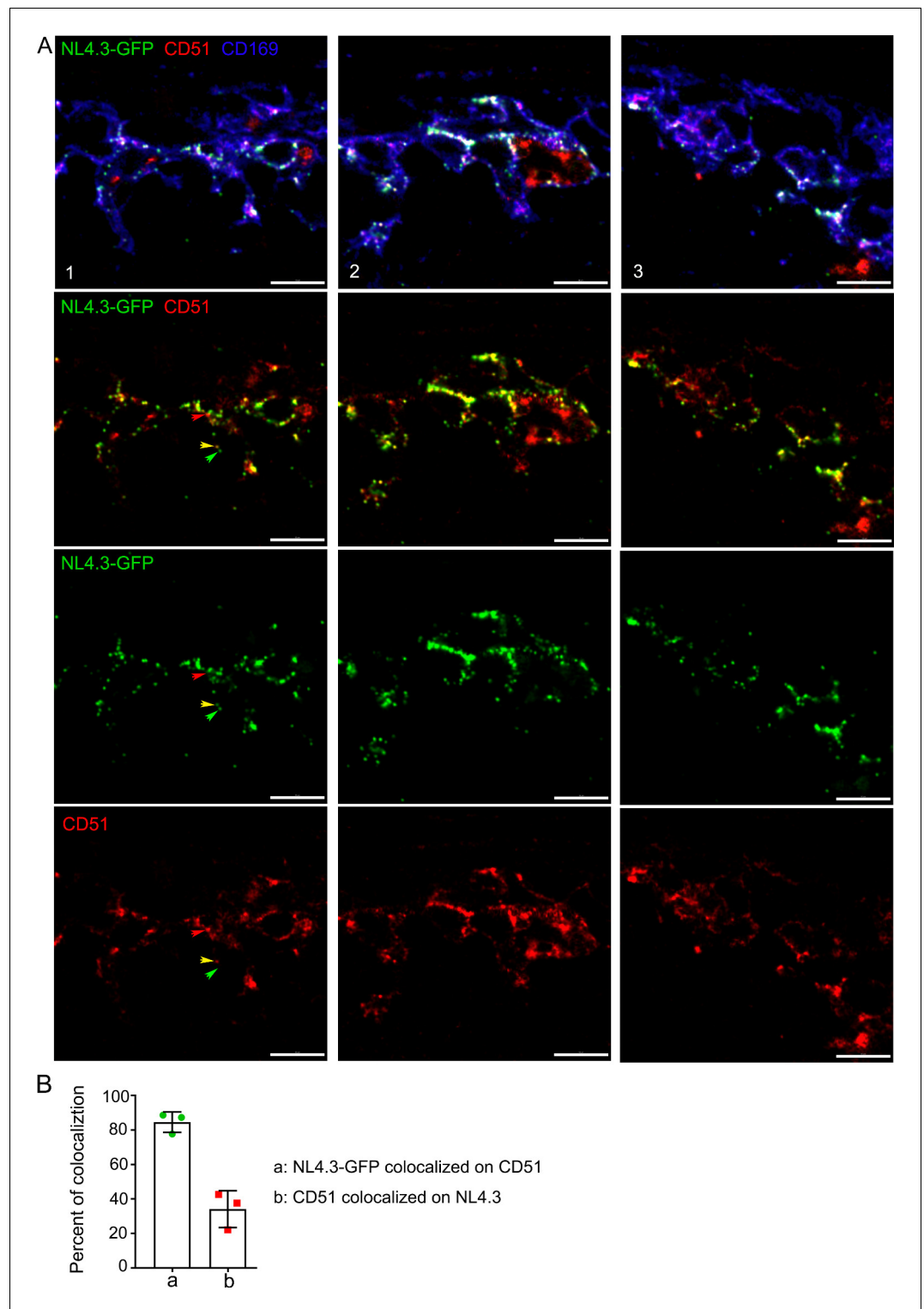


**Figure 3—figure supplement 2.** NL4.3-GFP VLPs colocalized with  $\alpha$ v integrins. (A) Confocal micrographs of NL4.3-GFP in inguinal LN harvested 1 hr after injection. Fixed sections were stained with PE-conjugated CD51 antibody (red) and CD169 antibody (blue). Three representative LN slices (columns 1, 2, and 3) are shown. Indicated signals in each row visualized. Yellow arrowhead indicates merged signal of NL4.3-GFP and CD51. Green and red arrowheads indicate internal negative control corresponding to CD51 and NL4.3-GFP. (B) Percent of colocalization between NL4.3-GFP and CD51 was analyzed and plotted. Scale bars 10  $\mu$ m (A).

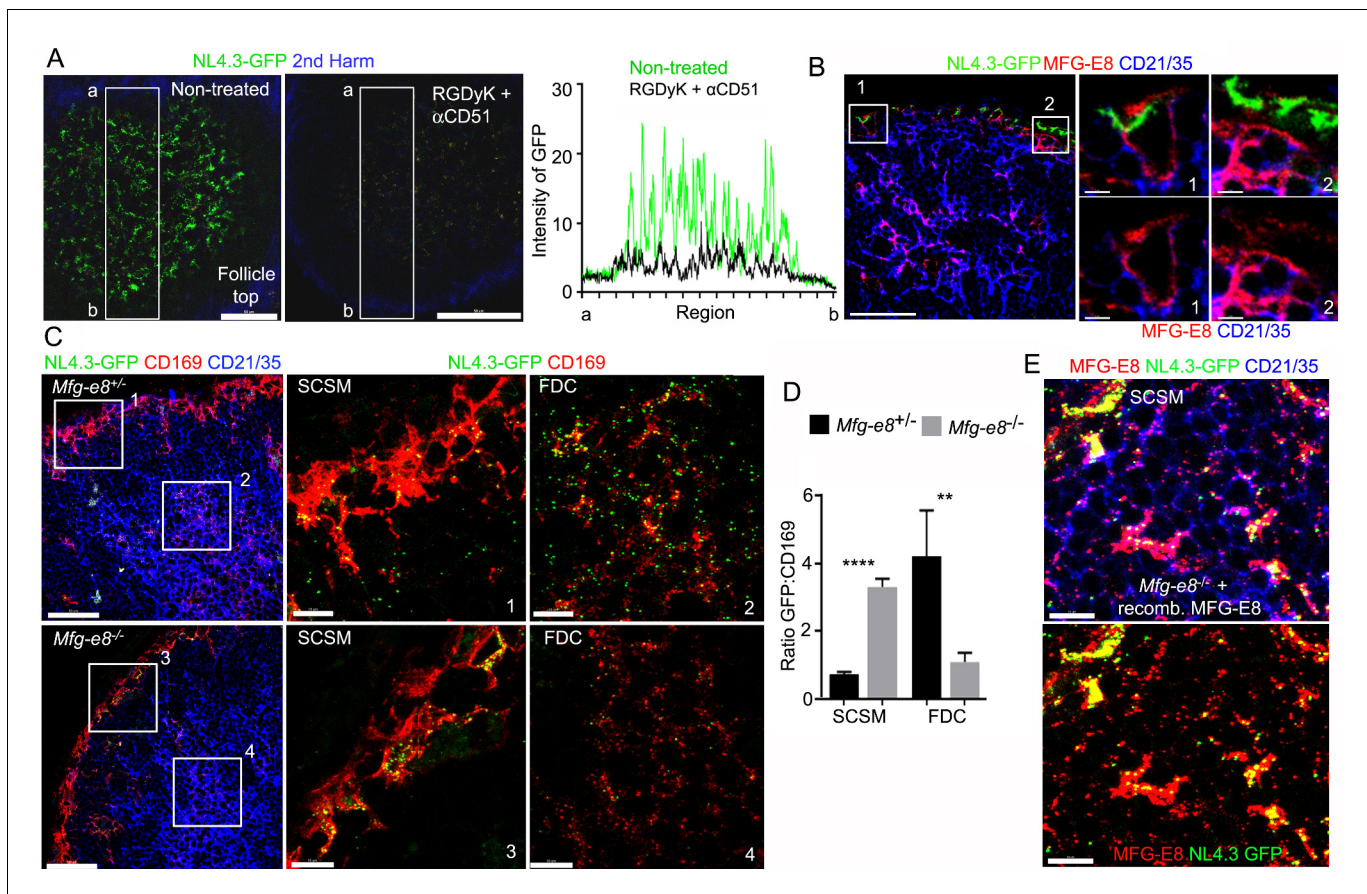


**Figure 4.** Requirement for  $\alpha$ v integrins and MFG-E8 to load NL4.3-GFP VLPs on the FDC network. (A) LN TP-LSM images from control or from RGDyK (100  $\mu$ g) + CD51 (10  $\mu$ g) blocking antibody treated mice captured 80 min after integrin blockade and 20 min after NL4.3-GFP injection. GFP intensity in delineated area shown in graph. (B) LN confocal micrographs of NL4.3-GFP from a mouse pretreated with RGDyK + CD51 blocking antibody as same in (A). LN collected 1 hr after VLPs injection. SCSMs (in Boxes) zoomed in middle and right panels. (C) Confocal micrographs of NL4.3-GFP in *Mfg-e8*<sup>+/-</sup> LN (upper) and *Mfg-e8*<sup>-/-</sup> LN (lower) 20 hr after VLPs injection. Boxes zoomed in middle and right panels. (D) Graph of NL4.3-GFP signal overlying SCSM and FDCs normalized to CD169<sup>+</sup> deposition signal. Four different sections analyzed and plotted. (E) Confocal micrographs of NL4.3-GFP and recombinant MFG-E8 in *Mfg-e8*<sup>-/-</sup> LN 3 hr after VLP injection. MFG-E8 injected 1 hr before NL4.3-GFP. Scale bars 50  $\mu$ m (A), 20  $\mu$ m and 5  $\mu$ m (B), 50  $\mu$ m and 10  $\mu$ m (C), and 10  $\mu$ m (E). \*\*,  $p < 0.01$ , \*\*\*\*,  $p < 0.0001$ .



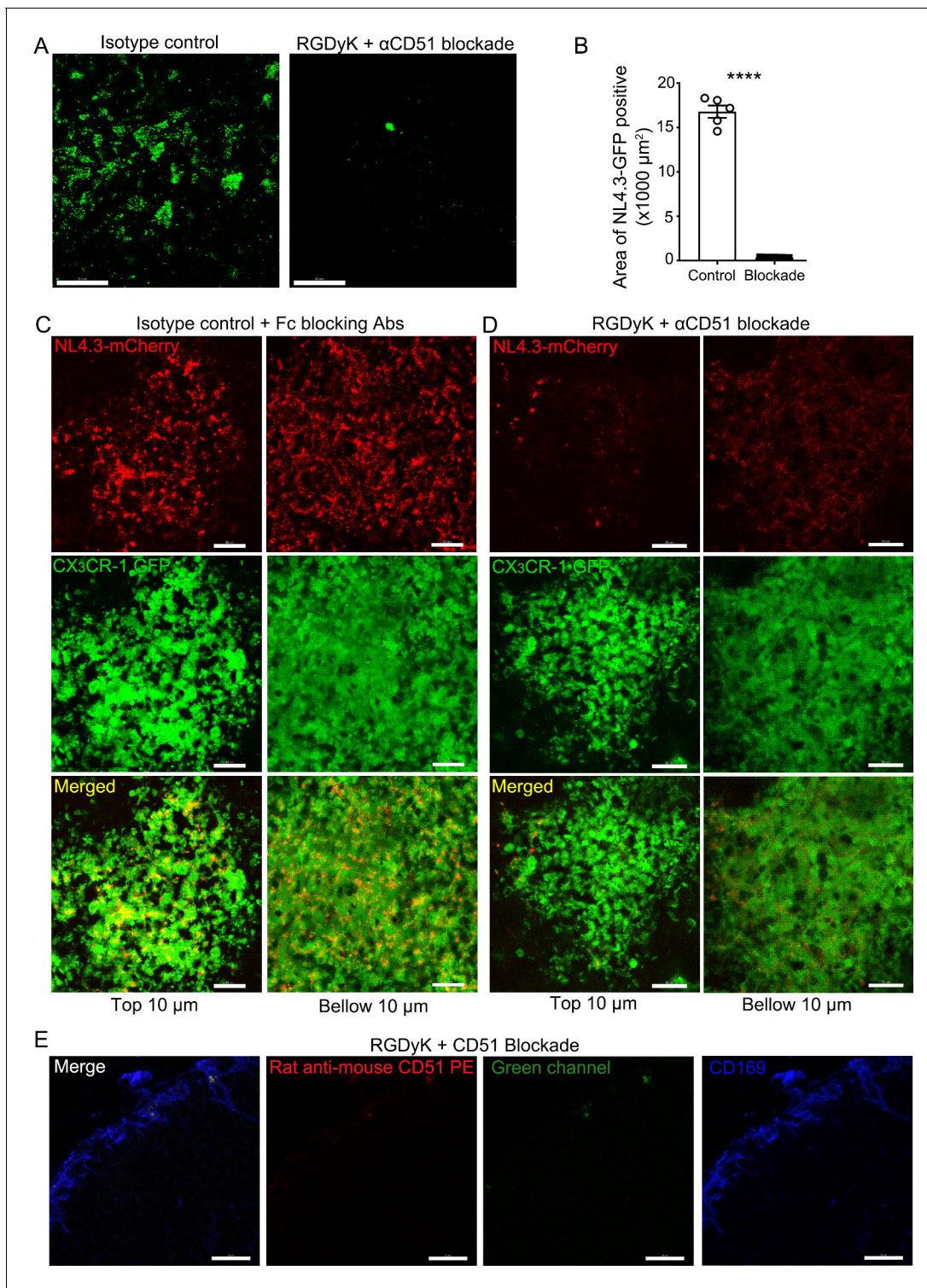


**Figure 4—figure supplement 1.** Integrin blockade inhibits VLP binding to SCSMs. (A) LN TP-LSM micrographs from isotype control (Rat IgG1<sub>k</sub>, 10  $\mu\text{g}$ ) or from RGDyK (100  $\mu\text{g}$ ) + CD51 (10  $\mu\text{g}$ ) blocking antibody treated mice captured 80 min after integrin blockade and 20 min after NL4.3-GFP injection. (B) NL4.3-GFP<sup>+</sup> capsular area was measured and plotted. Five different area from two different experiments analyzed. \*\*\*\*;  $p < 0.0001$ . (C) LN TP-LSM micrographs of CX<sub>3</sub>CR-1-GFP mice from isotype control (Rat IgG1<sub>k</sub>, 10  $\mu\text{g}$  plus Fc blocking antibody, 10  $\mu\text{g}$ ) antibody treated mice. Images were captured 1 hr after antibodies and NL4.3-mCherry simultaneous injection. (D) LN TP-LSM micrographs of CX<sub>3</sub>CR-1-GFP mice from RGDyK (100  $\mu\text{g}$ ) + CD51 (10  $\mu\text{g}$ ) blocking antibody treated mice. Images were captured 1 hr after integrin blockade and NL4.3-mCherry simultaneous injection. In C and D, left column visualized initial 10  $\mu\text{m}$  thick volume image of SCSM layer. Right column visualized subsequent 10  $\mu\text{m}$  thick volume image of SCSM layer. Figure 4—figure supplement 1 continued on next page

Figure 4—figure supplement 1 continued

(E) Confocal micrographs of inguinal LN from a mouse pretreated for 2 hr with RGDyK + CD51 blocking antibody. Fixed section was stained with PE-conjugated anti-mouse CD51 antibody (red) and CD169 antibody (blue). Left panel, all signals merged. Second panel, red signal only. Third panel, green signal only. Fourth panel, CD169 signal only. Scale bars 30  $\mu\text{m}$  (A, C, D), 20  $\mu\text{m}$  (E).

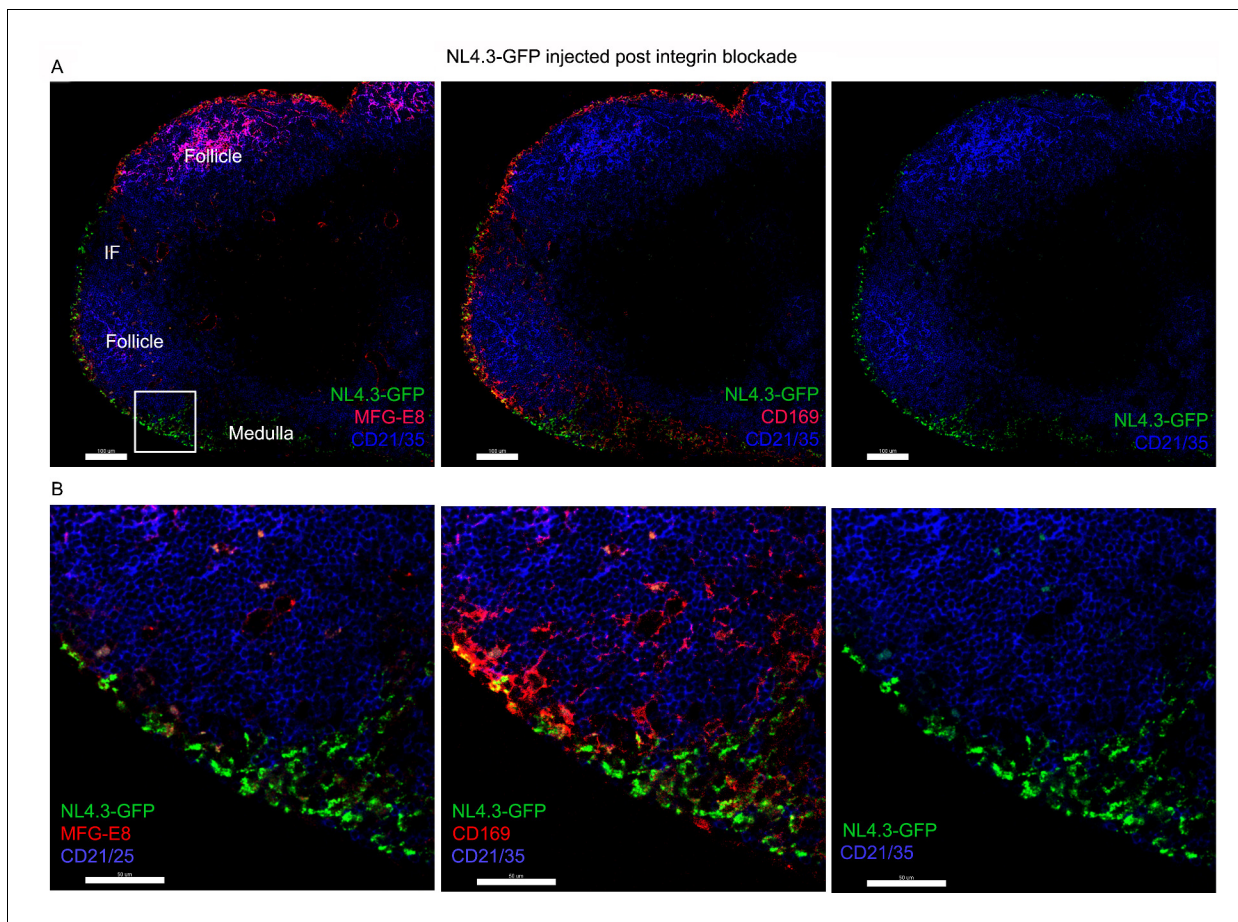


**Figure 4—figure supplement 2.** Integrin blockade shifts VLP targeting to the medullary SMs and strongly reduces FDC loading. **(A)** Confocal micrographs of NL4.3-GFP (green) in inguinal LN from a mouse pretreated for 1 hr with RGDyK + CD51 blocking antibody. The LN was harvested 1 hr after VLPs injection. Top panels show CD21/35 and NL4.3-GFP signals. The left panel also shows MFG-E8 and the middle panel CD169. B cell follicle (follicle) and area (medulla) are indicated. **(B)** Box (cortical/medullary junction) in left, above micrograph electronically zoomed and shown with indicated signals. Scale bars 100  $\mu$ m (A), 50  $\mu$ m (B).



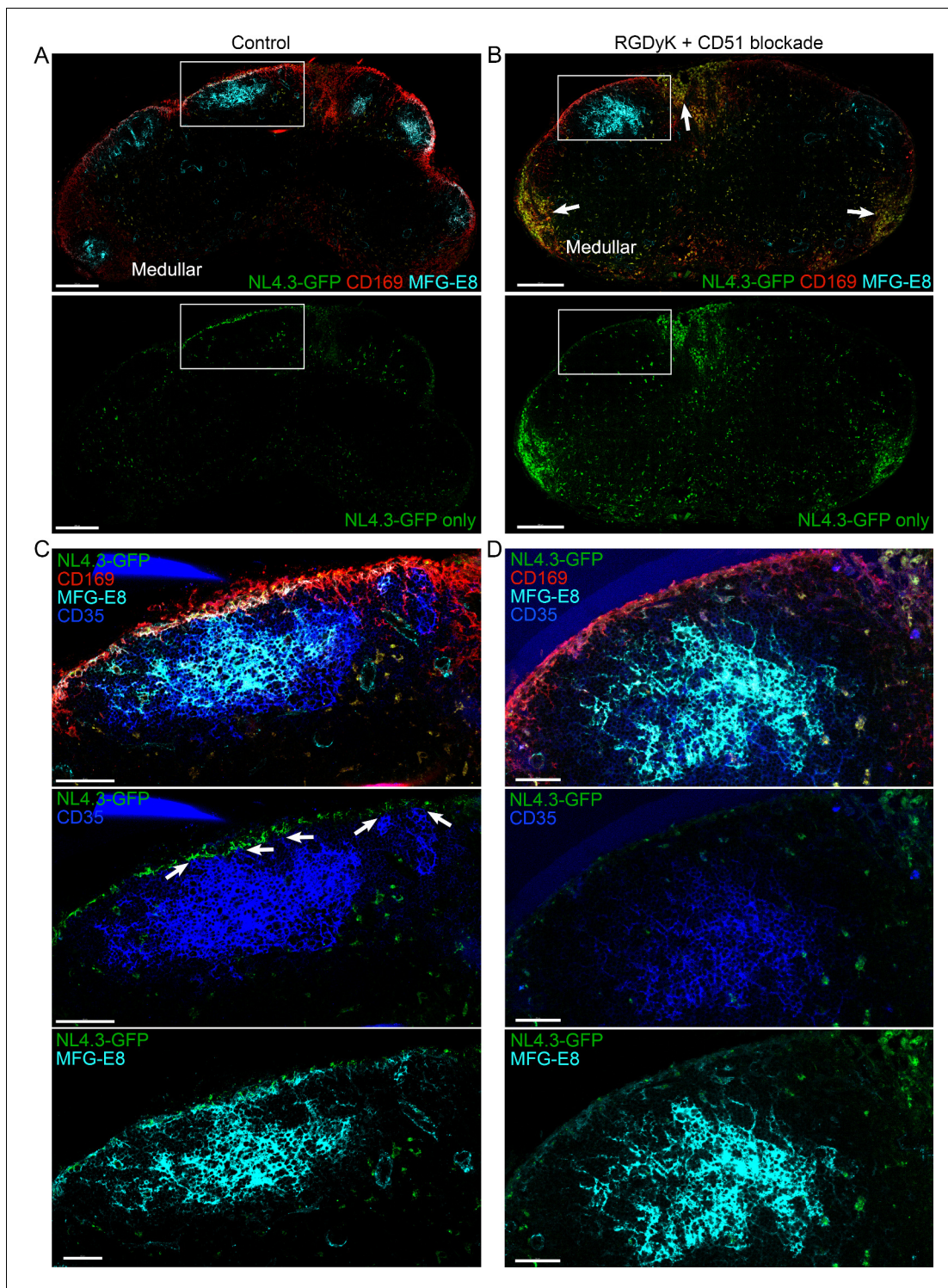


**Figure 4—figure supplement 3.** Integrin blockade shifts VLP targeting to the medullary SMs and strongly reduces FDC loading. (A) Confocal micrographs of NL4.3-GFP (green) in inguinal LN from a mouse pretreated for 5 hr with isotype control antibody (Rat IgG1<sub>k</sub>, 10  $\mu$ g). The LN was harvested 1 hr after VLPs injection. Upper panel show CD169, MFG-E8 and NL4.3-GFP signals. Lower panel show NL4.3-GFP signal only. (B) Confocal micrographs of NL4.3-GFP (green) in inguinal LN from a mouse pretreated for 5 hr with RGDyK + CD51 blocking antibody. The LN was harvested 1 hr after VLPs injection. Upper panel show CD169, MFG-E8 and NL4.3-GFP signals. Lower panel show NL4.3-GFP signal only. Arrows indicates medullary area in LN. (C, D) Box in A and B electronically zoomed and shown with indicated signals in C and D. Arrows of middle panel in C indicate MFG-E8<sup>+</sup> compartment as direct contact point between SCSM and FDC. Scale bars 200  $\mu$ m (A, B), 50  $\mu$ m (C, D).

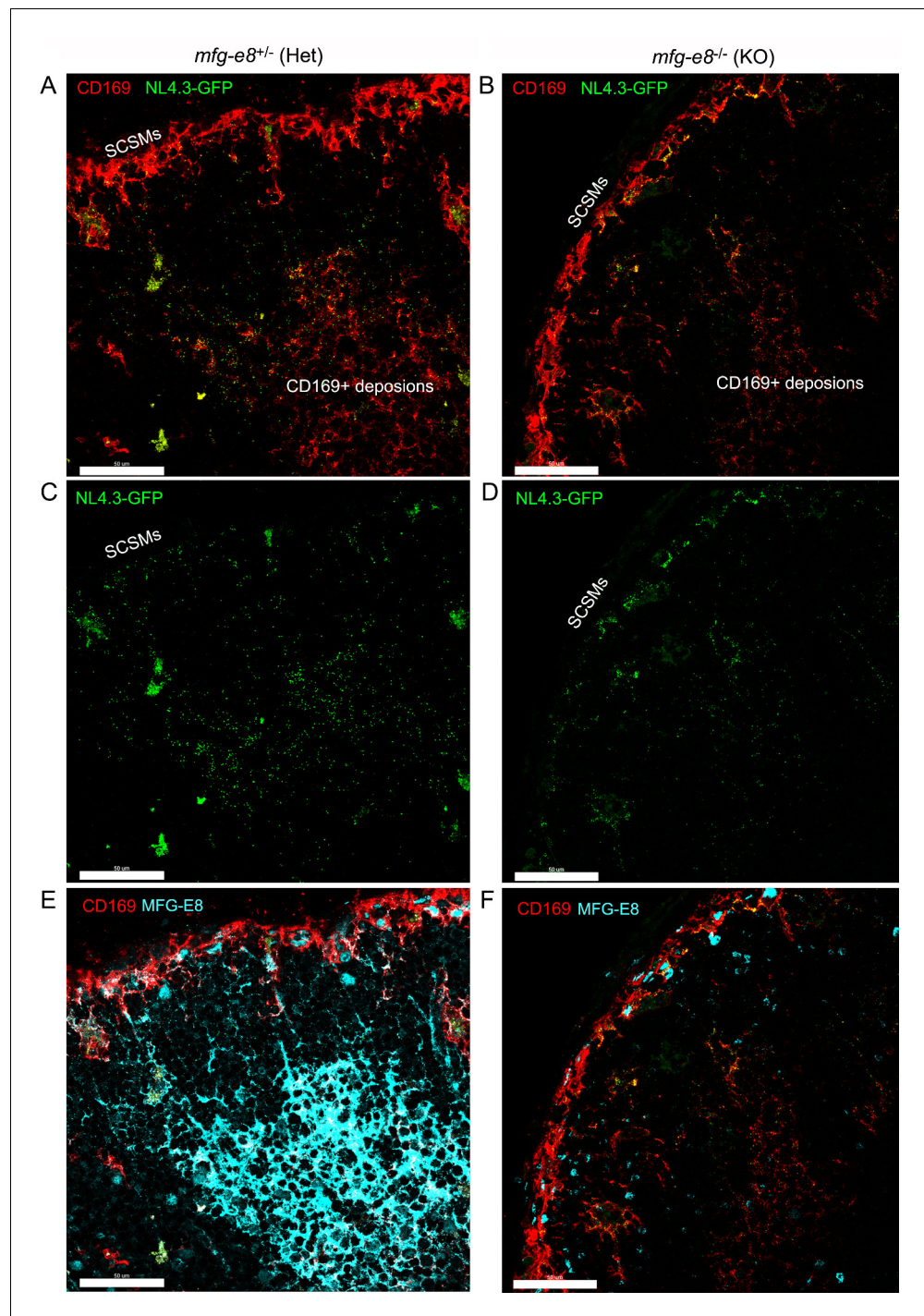


**Figure 4—figure supplement 4.** In *Mfg-e8<sup>-/-</sup>* LNs HIV-1-VLPs accumulate on the SCSMs yet poorly load the FDC network. (A, B) Confocal micrographs of NL4.3-GFP (green) in inguinal LN obtained from *Mfg-e8<sup>+/-</sup>* mouse (left column) and *Mfg-e8<sup>-/-</sup>* mouse (right). LN was harvest 20 hr after VLPs injection. CD169<sup>+</sup> depositions on FDC network are indicated. (C, D) Images shown without CD169 signal. (E, F) Images show MFG-E8 expression. Scale bars 50 μm.



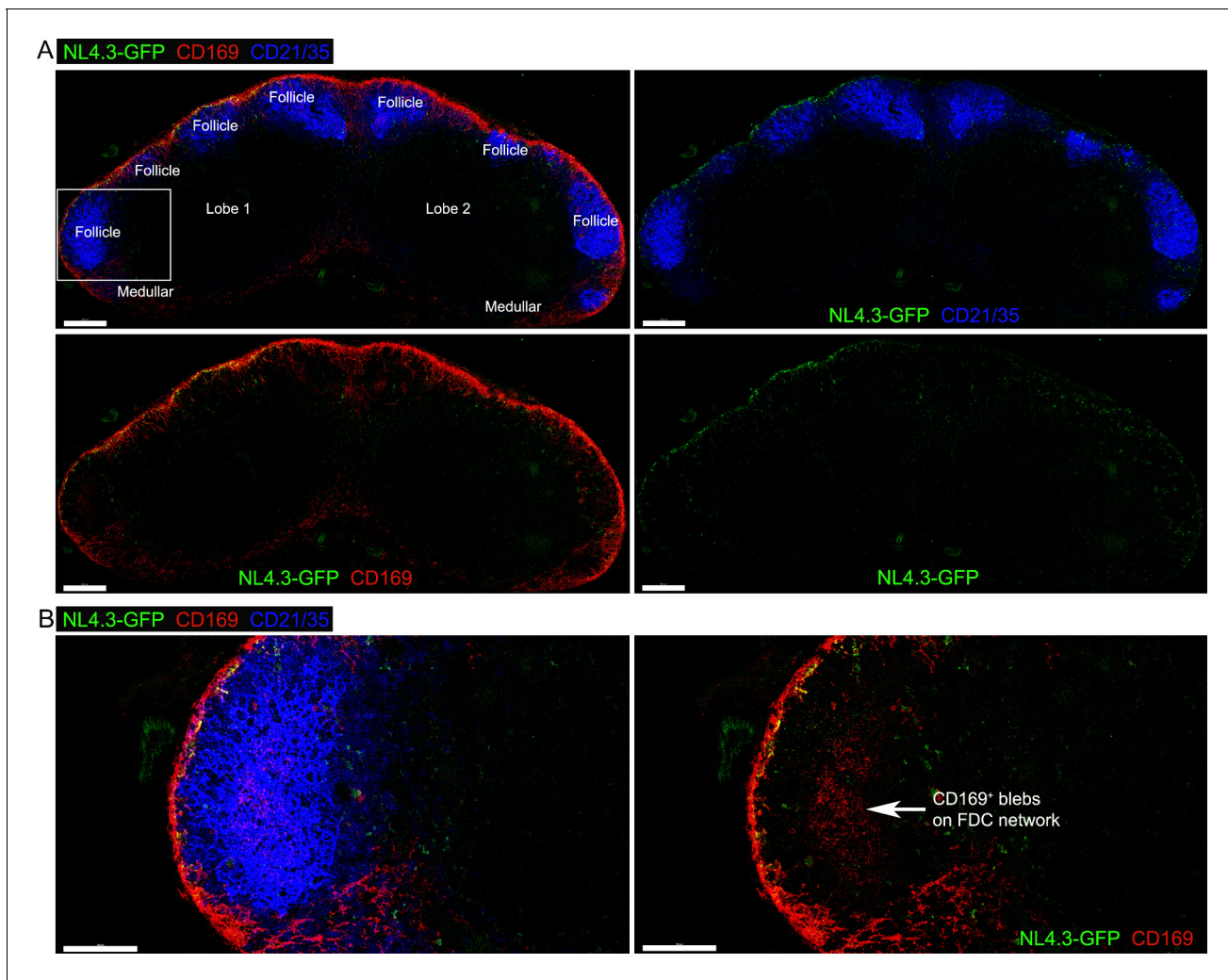


**Figure 4—figure supplement 5.** The deposition of CD169<sup>+</sup> blebs on FDCs in the middle of B cell follicle. (A) Tiled confocal micrographs of NL4.3-GFP in inguinal LN harvested 1 hr after injection. Fixed LN section was stained with antibodies of CD169 (red) and CD21/35 (blue). Two separated lobes (lobe 1 and lobe 2) in inguinal LN are indicated. Left upper panel, B cell follicles (Follicle) and medullary area (Medullar) are indicated. Left lower panel, NL4.3-GFP and CD169 signals. Right upper panel, NL4.3-GFP and CD21/35 signals. Right lower panel, NL4.3-GFP signal only. (B) Boxed B cell follicle in (A) was electronically zoomed, left. Deposition of CD169<sup>+</sup> blebs on center of FDC network indicated by arrow, right. Scale bars 200  $\mu$ m (A) and 100  $\mu$ m (B).

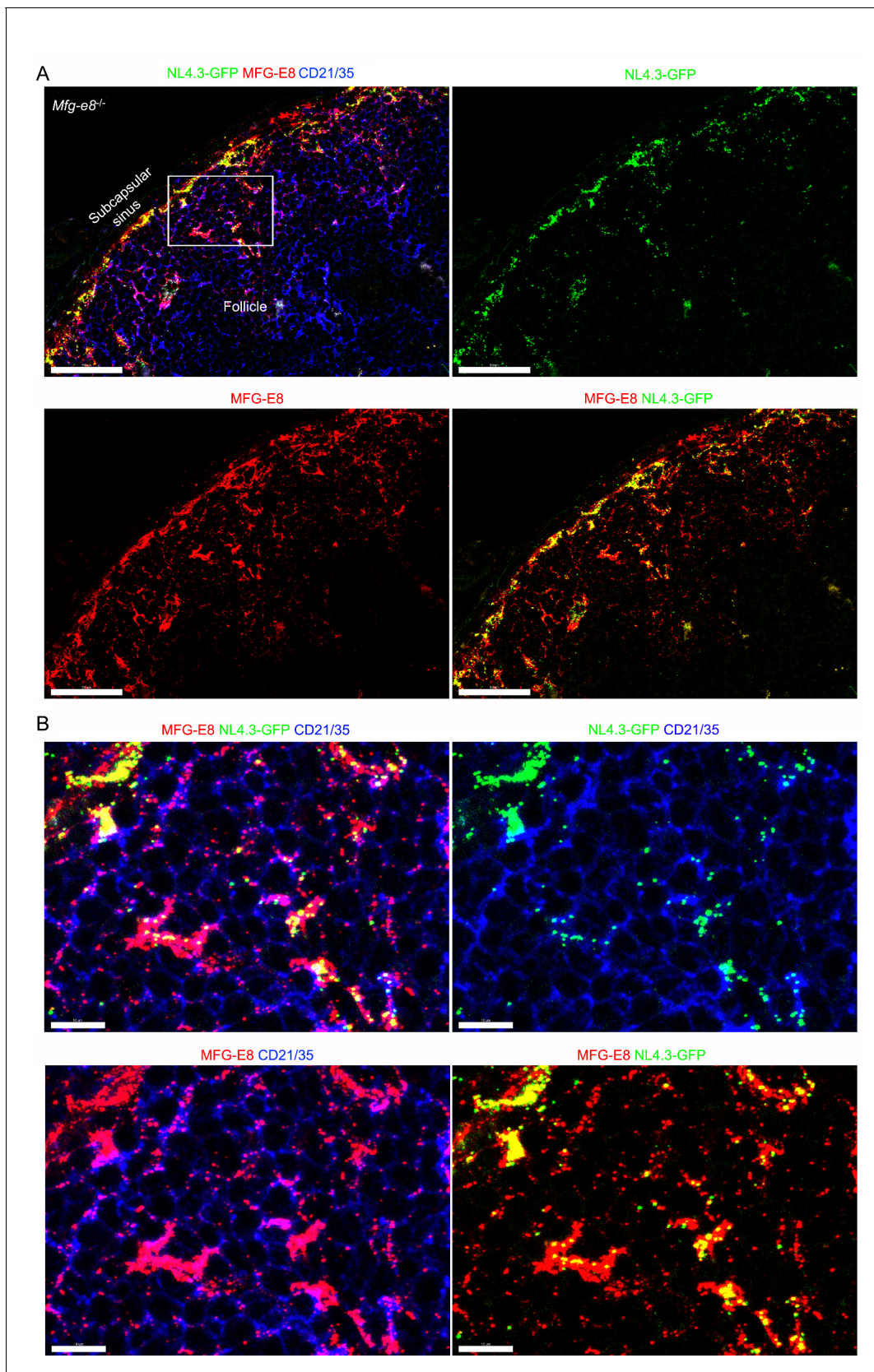


**Figure 4—figure supplement 6.** Recombinant MFG-E8/NL4.3-GFP complexes captured by SCSM and subsequently translocated to FDC network. (A) Confocal micrographs of NL4.3-GFP and recombinant MFG-E8 in the inguinal LN following injection into a *Mfg-e8*<sup>-/-</sup> mouse. The LN was harvested after Figure 4—figure supplement 6 continued on next page



*Figure 4—figure supplement 6 continued*

3 hr after recombinant MFG-E8/NL4.3-GFP complex injection. MFG-E8 detected by antibody staining. The indicated signals are shown in the separate panels. **(B)** Box from panel A was electronically zoomed (top, left). NL4.3-GFP and CD21/35 signals shown (top, right). MFG-E8 and CD21/35 signals shown (bottom, left). MFG-E8 and NL4.3-GFP signal shown (bottom, right). Scale bars 50  $\mu\text{m}$  (**A**), 10  $\mu\text{m}$  (**B**).

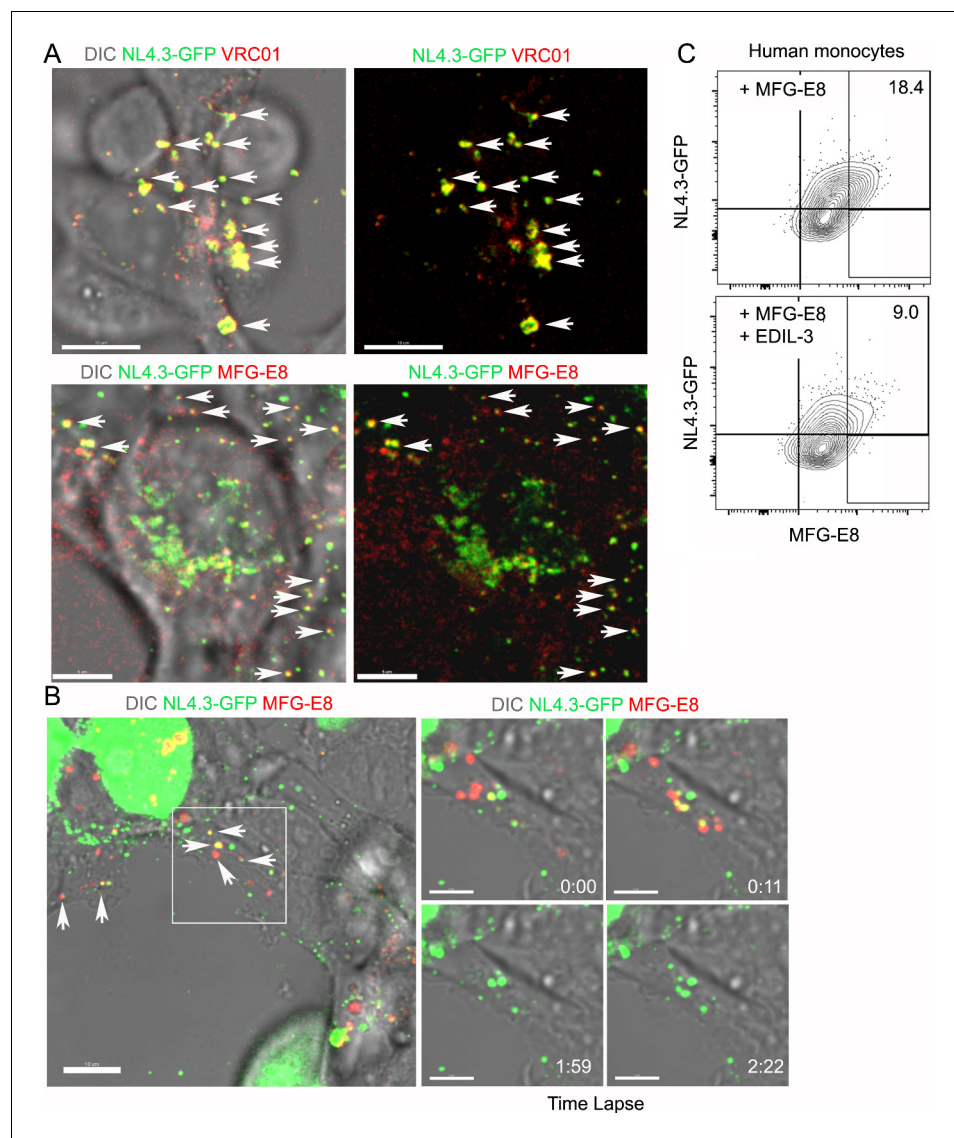


**Figure 5.** MFG-E8/NL4.3-GFP complexes present in transfected HEK293T cell cultures. **(A)** Confocal image from live cell imaging of HEK293T cell previously transfected with NL4.3-GFP plasmid. NL4.3-GFP detected by VRC01 staining (upper row). MFG-E8 detected by antibody staining (lower row). Left image includes DIC image. Arrows indicate merged signal. **(B)** Confocal image from live cell imaging of HEK293T cell previously transfected NL4.3-GFP plasmid. Labeled recombinant MFG-E8 was added to the cells prior to imaging. MFG-E8 bound NL4.3-GFP virions are indicated (arrows). The box in the left panel was electronically zoomed at four different time points. **(C)** Flow cytometry indicates competitive inhibition of EDIL-3 to MFG-E8 mediated NL4.3-GFP binding on human monocytes. Scale bar 5  $\mu$ m (A), 10 and 5  $\mu$ m (B).

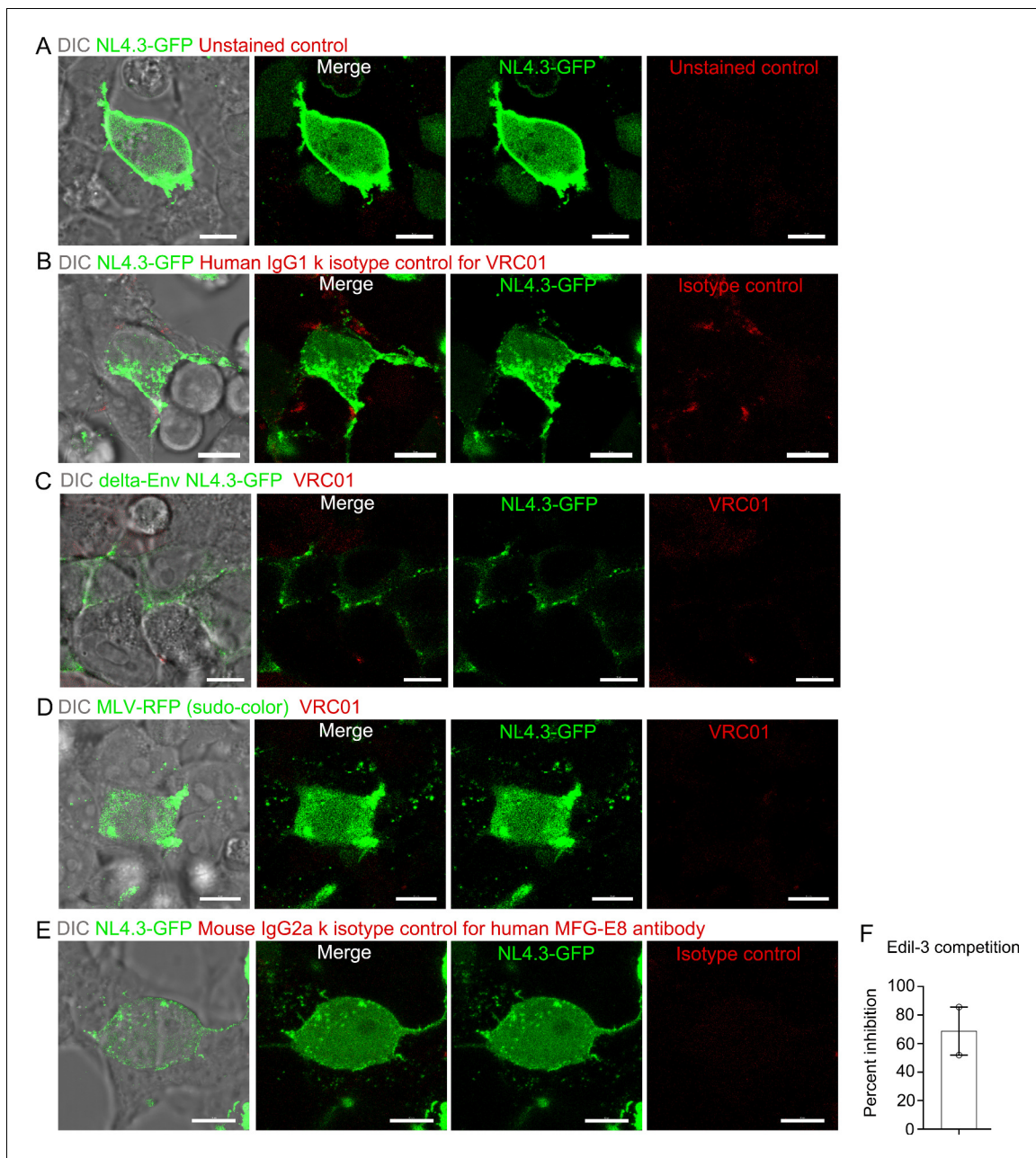


**Figure 5—figure supplement 1.** Isotype Controls for HEK293T imaging and Edil-3 competition to MFG-E8 binding on NL4.3-GFP VLPs. Confocal micrographs from live cell imaging of HEK293T cell previously transfected with NL4.3-GFP plasmid. First panel merged with DIC and fluorescence signals. Other panels shown with indicated signals. (A) Micrographs shown unstained control for antibodies. (B) Micrographs shown isotype control (human IgG1<sub>k</sub>) stain for VRC01 (C) Micrographs from live cell imaging of HEK293T cell previously transfected with delta-Env NL4.3-GFP plasmid. Micrographs shown VRC01 antibody stain. (D) Micrographs from live cell imaging of HEK293T cell previously transfected with pSV-A-MLV-env, pSV-Ψ-MLV-env and MLV Gag-RFP. Micrographs shown VRC01 antibody stain. (E) Micrographs shown isotype control (mouse IgG2a<sub>k</sub>) stain for human MFG-E8 antibody. (F) Percent inhibition by recombinant Edil-3 of recombinant MFG-E8 binding to NL4.3-GFP VLPs is plotted. Results from two separated experiments. Scale bars 10 μm.



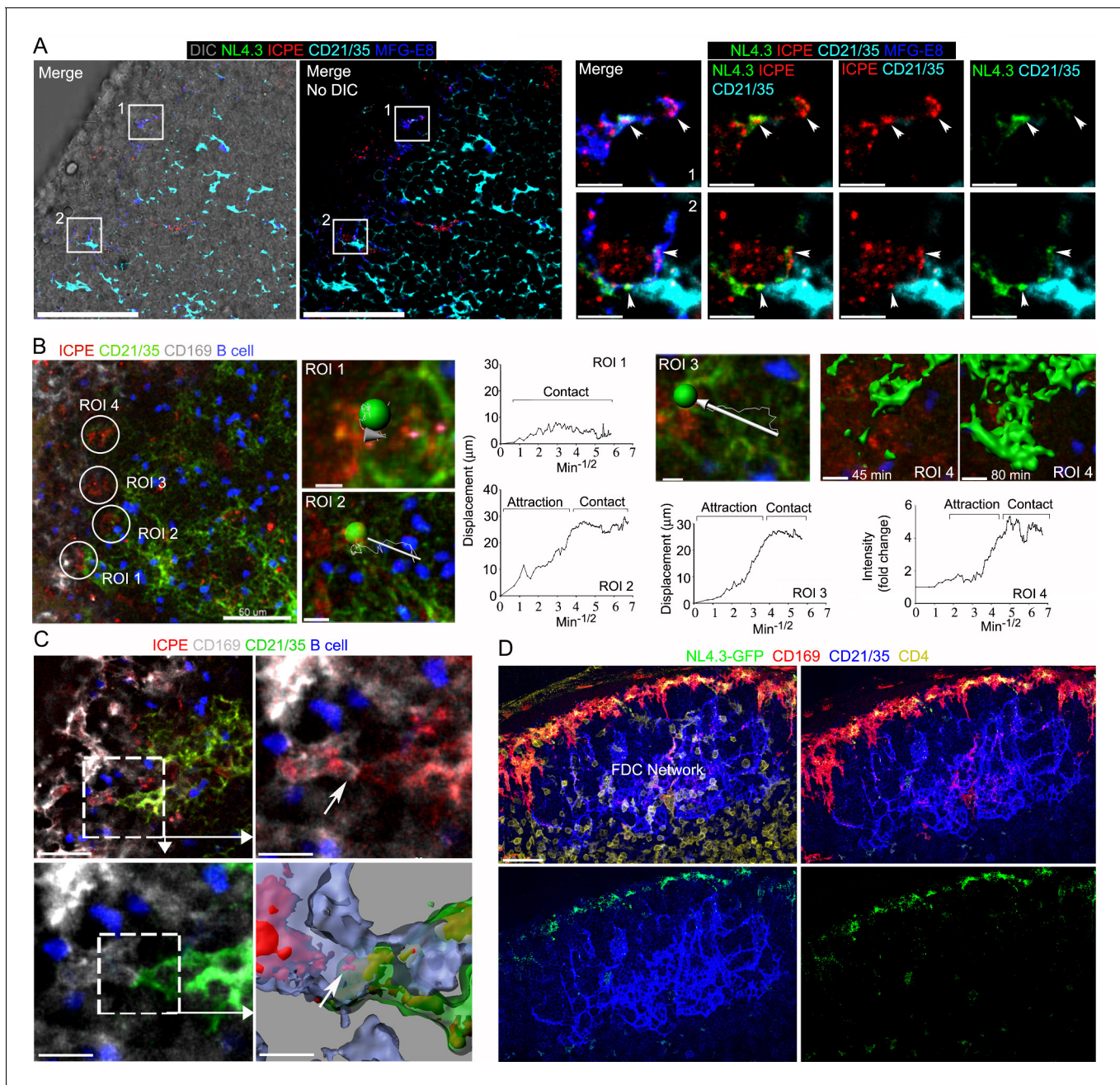


**Figure 6.** Immune complexes co-localize with HIV-1 VLPs on SCSMs and trigger the transient abutment of FDCs and SCSMs. (A) LN confocal micrographs of NL4.3-GFP and ICPE 4 hr after NL4.3-GFP injection. ICPE injected 1.5 hr after NL4.3-GFP. In left panel DIC superimposed image shown. SCSMs in boxes (left and middle panels) zoomed. Arrows indicate NL4.3-GFP, ICPE, and MFG-E8 co-localization. (B) LN TP-LSM image following ICPE injection. In ROI 1–3 arrows show FDC displacement and green balls indicate arbitrary center points of FDC tracked. Graphs show FDC movement relative to SCSM. ROI4 shown as 3D-reconstructed volume of a FDC at indicated times. Graph records time-dependent changes in FDC signal. (C) LN TP-LSM images at SCSM/FDC interface 3 hr after ICPE injection. Dotted white box zoomed in top, right and bottom, left panels. Dotted box reconstructed as 3D-volume, bottom right. Arrows indicate an abutment of SCSM and FDC, which contains ICPE. (D) Confocal images of LN sections showing impact of pertussis toxin on FDC network translocation. Pertussis toxin (500 ng) injected 2 hr before NL4.3-GFP. LN analyzed 6 hr later. Scale bars 50 and 5  $\mu\text{m}$  (A), 50 and 5  $\mu\text{m}$  (B), 30 and 10  $\mu\text{m}$  (C), and 30  $\mu\text{m}$  (D).



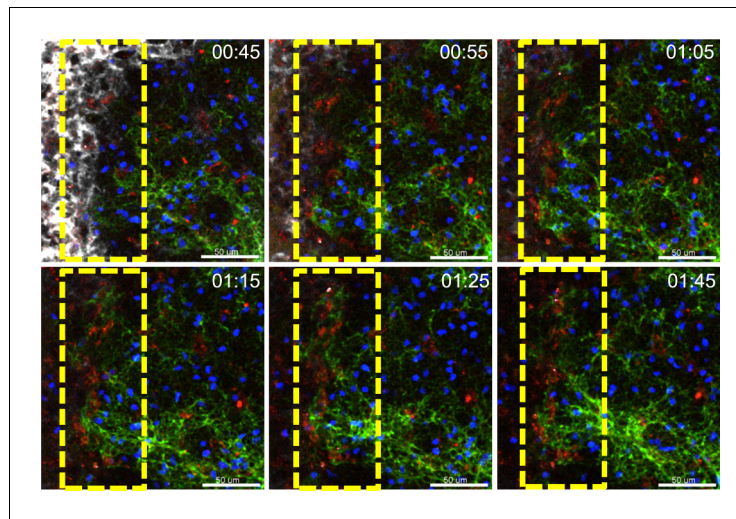


**Figure 6—figure supplement 1.** A dynamic FDC network shift towards SCSMs. TP-LSM images from the inguinal LN from 45 min to 1 hr 45 min after injection of ICPE (red). Dotted yellow box indicates interface between SCSMs and FDCs network revealed by injected CD169 (white) and CD21/35 (green) antibodies. B cells (blue) adoptively transferred the previous day outline the follicle. Time stamp indicates time after ICPE injection, hour:min. Scale bars 50  $\mu$ m.

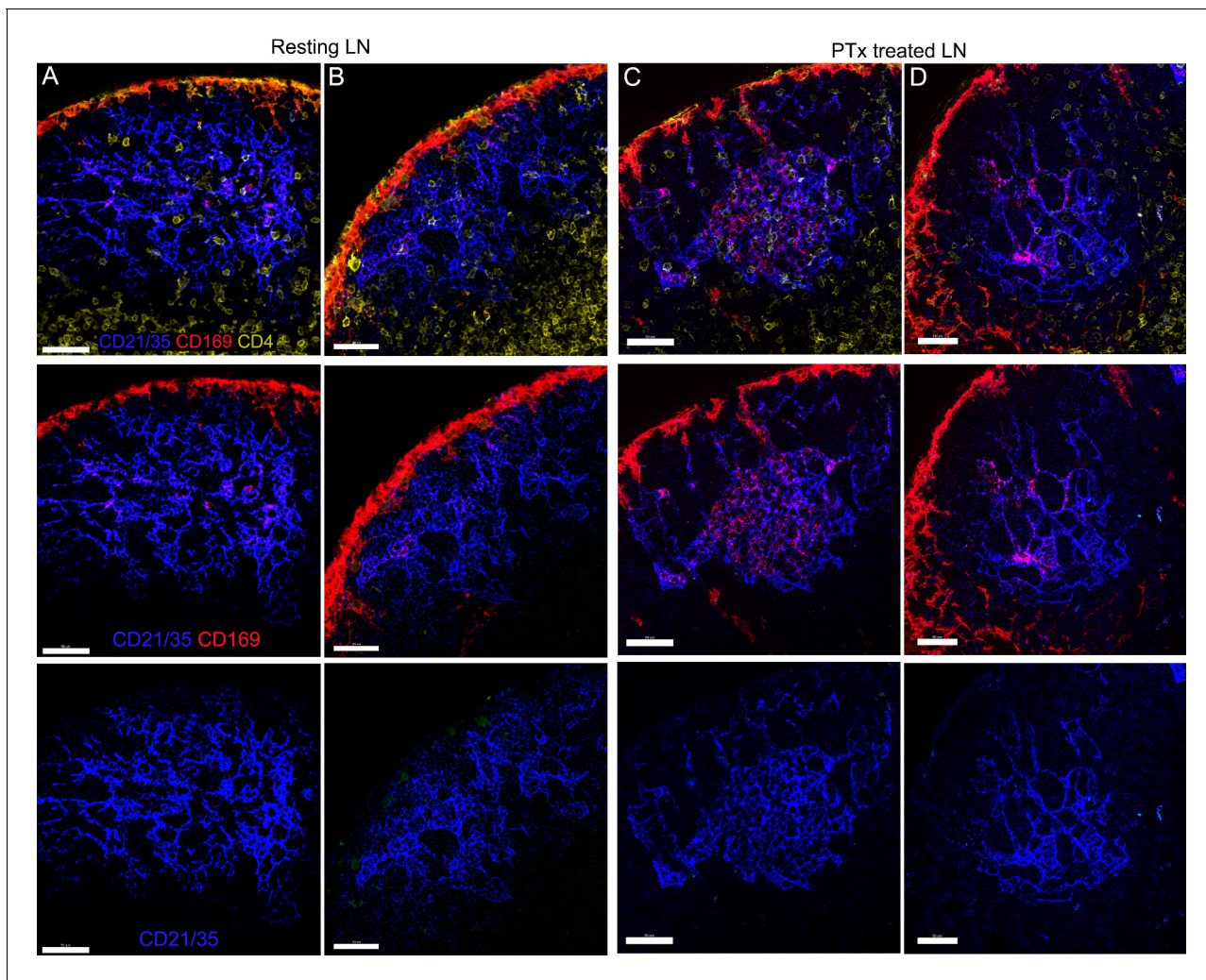


**Figure 6—figure supplement 2.** The impact of pertussis toxin on FDC network localization in B cell follicle. Confocal micrographs of LN sections showing FDC network location in B cell follicles. Resting LN (A and B) indicates that lymph node collected without treatment. PTx treated LN (C and D) indicates that lymph node collected at 8 hr post treatment of Pertussis toxin (500 ng). CD169 (red) visualized SCSMs overlaying capsule of B cell follicle. CD4 (yellow) stain delineated follicular border to T cell zone. FDCs (blue) were visualized by CD21/35 stain. Signals in each row indicated column A. Scale bars 50 μm.

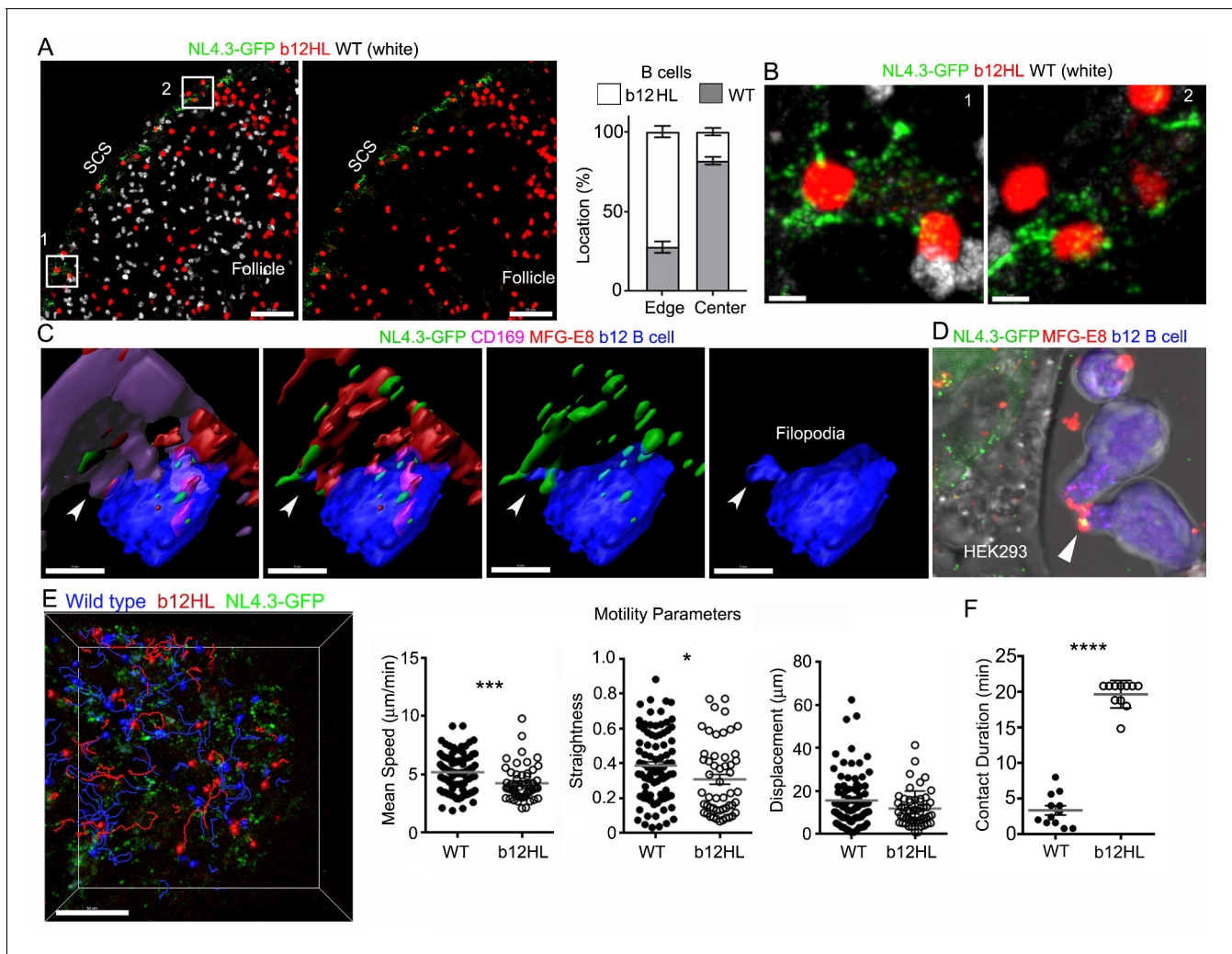


**Figure 7.** gp120-specific B cells extract HIV-1 VLPs from SCSMs. (A) LN confocal images of adaptively transferred b12 and wild type B cells 3 hr after NL4.3-GFP injection. B cells transferred day before. Right panel shows only b12 B cells in the follicle. Graphical analysis shows percent ratio of wild type versus b12 B cells in B cell follicle center (Center) and follicular edge (Edge). (B) Boxes (1 and 2) in right panel zoomed. (C) 3D-reconstructed images of b12 B cell tightly associated with NL4.3-GFP bearing SCSMs. Arrows indicate an MFG-E8<sup>+</sup> compartment on SCSM. Final panel shows a b12 B cell filopodia probing MFG-E8<sup>+</sup> compartment. (D) Confocal image from live cell imaging of HEK293T cell previously transfected with NL4.3-GFP plasmid. Directly labeled recombinant MFG-E8 (red) was added 1 hr prior to imaging. Arrow indicates MFG-E8 binding NL4.3-GFP VLP. (E) TP-LSM image overlaid with the tracks of wild type (blue) and b12 B cells (red). B cells were adoptively transferred 1 day before NL4.3-GFP VLP injection. 1 hr after NL4.3-GFP injection intravital images were taken and used to analyze B cells behavior. (F) Motility parameters were calculated and shown. A comparison between contact durations between B cells (WT or b12 B cells) and VLP bearing SCSM are shown (right panel). Scale bars 50  $\mu\text{m}$  (A), 5  $\mu\text{m}$  (B), 5  $\mu\text{m}$  (C), and 50  $\mu\text{m}$  (E). \*,  $p < 0.1$ , \*\*,  $p < 0.01$ , \*\*\*\*,  $p < 0.0001$ .